Adiabatic reduction of circulation-related CO_2 air-sea flux biases in a North Atlantic carbon-cycle model

Carsten Eden[1] and Andreas Oschlies[2]

Received 1 April 2005; revised 6 December 2005; accepted 19 January 2006; published 11 May 2006.

[1] Physical transport processes of carbon, alkalinity, heat, and nutrients to a large extent control the partial pressure of CO_2 at the sea surface and hence the oceanic carbon uptake. Using a state-of-the-art biogeochemical model of the North Atlantic at eddy-permitting resolution we show that biases in the simulated circulation generate errors in air-sea fluxes of CO_2 which are still larger than those associated with the considerable uncertainties in parameterizations of the air-sea gas exchange. A semiprognostic correction method that adiabatically corrects the momentum equations while conserving water mass properties and tracers is shown to yield a more realistic description of the carbon fluxes into the North Atlantic at little additional computational cost. Owing to upper ocean flow patterns in better agreement with observations, simulated CO_2 uptake in the corrected regional model is larger by 25% compared to the uncorrected model.

Citation: Eden, C., and A. Oschlies (2006), Adiabatic reduction of circulation-related CO_2 air-sea flux biases in a North Atlantic carbon-cycle model, *Global Biogeochem. Cycles*, *20*, GB2008, doi:10.1029/2005GB002521.

1. Introduction

[2] At present, less than half of the total fossil-fuel and cement-manufacturing emissions of CO_2 accumulate in the atmosphere, with the remainder being attributed to sinks given by the ocean and terrestrial ecosystems [*Prentice et al.*, 2001]. To achieve reliable assessments of how Earth's climate will change in response to human CO_2 emissions, the fate of the anthropogenic CO_2 and the climate sensitivity of its present storage reservoirs needs to be understood. In a recent compilation of inorganic carbon measurements, *Sabine et al.* [2004] estimated that the ocean has taken up 48% of the total anthropogenic CO_2 released since the beginning of the industrial period. Such observational estimates, that have to calculate the relatively small (typically less than 5%) anthropogenic contribution from the measured total dissolved inorganic carbon, rely on a number of assumptions. Most crucial among them are steady states of the circulation, the marine biology and the air-sea pCO_2 disequilibrium as well as negligible diapycnal transport and correct tracer-based water mass age estimates. Certainly, none of these assumptions are exactly valid although the associated errors in the observational estimates are as yet difficult to quantify. However, for a section in the eastern Atlantic, where mixing rates are low and where methods should work relatively well, *Wanninkhof et al.* [1999] find that anthropogenic CO_2 inventories estimated by different methods agree only within 20% overall, with much larger regional variations.

[3] Numerical ocean general circulation models coupled to some kind of carbon chemistry model are a complementary approach to estimate the oceanic uptake of anthropogenic CO_2. Besides allowing for estimates of present-day budgets and fluxes, such dynamical models have the additional advantage that they can be used to study "what-if" scenarios and to make predictions for various scenarios into the future. Models do, however, have considerable errors that are also difficult to quantify: Various model studies like the Ocean Carbon-cycle Model Intercomparison Project (OCMIP-1/2) reveal large intermodel differences in the regional patterns of storage and fluxes of anthropogenic CO_2 [*Orr et al.*, 2001]. Because of the way OCMIP was designed, any model-model variations in that study simply reflect differences in the simulated physical circulation which have recently been investigated in more detail by *Doney et al.* [2004]. By comparing the simulated physics to observational data sets they identify several model biases that essentially all OCMIP-2 models have in common, such as too broad and displaced western boundary currents and therefore dislocated or even nonexisting subpolar frontal systems. These severe model biases lead to the large range of simulated total air-sea carbon flux patterns and in consequence to a large uncertainty in simulated oceanic uptake of anthropogenic CO_2.

[4] Many problems of the relatively coarse-resolution carbon cycle models (with lateral grid spacings of a few degrees) are generally thought to disappear when increasing the grid resolution. This "brute force" approach has indeed shown some success for physical models [*Smith et al.*, 2000; *Chassignet and Garraffo*, 2001; *Oschlies*, 2002; *Eden and Böning*, 2002]. However, even results of state-of-the-art eddy resolving models (with grid spacings of a few kilometers) are sensitive to model details such as the parameterization of sub-grid-scale mixing or interaction with

[1]Leibniz Institute for Marine Science at University of Kiel (IFM-GEOMAR), Kiel, Germany.
[2]National Oceanography Centre, Southampton, UK.

0886-6236/06/2005GB002521

topography, pointing to (possibly yet unresolved) processes not well understood. Notorious deficiencies in the Atlantic Ocean include the separation and downstream path of the Gulf Stream [*Chassignet and Garraffo*, 2001] and the location of the subpolar front in the western North Atlantic [*Willebrand et al.*, 2001; *Eden et al.*, 2004]. In addition, the costs to integrate such global eddy-resolving models with very high horizontal resolution coupled to biogeochemical models at timescales longer than decades will still exceed available computing resources for the near future.

[5] In order to reduce errors in the circulation field and to avoid the ocean model drifting too far away from the observations, some carbon cycle models include subsurface restoring terms for temperature and salinity [*Aumont et al.*, 1999; *LeQuere et al.*, 2000]. This approach is sometimes called ''robust diagnostic'' [*Sarmiento and Bryan*, 1982]. Besides other serious problems as discussed by *Greatbatch et al.* [1991] and *Ezer and Mellor* [1994], the robust diagnostic method introduces unphysical diabatic terms and associated artificial diapycnal transports of passive tracers. While still conserving tracers other than temperature and salinity globally, this generates spurious tracer sources and sinks on individual isopycnals.

[6] In the present study we apply a more satisfactory method for correcting the simulated flow field. This so-called ''semiprognostic'' method [*Sheng et al.*, 2001] applies a correction of the horizontal pressure gradient in the horizontal momentum equations. The correction is calculated from hydrographic observations but does not directly affect tracer budgets, including those of temperature and salinity. The method is therefore adiabatic and conserves tracer and water mass properties. It has been shown to greatly improve the circulation and surface heat fluxes in a state-of-the-art eddy-permitting model of the North Atlantic [*Eden et al.*, 2004]. In the following, we use essentially the same physical model as *Eden et al.* [2004], but this time augmented by a biogeochemical tracer model, to demonstrate that the adiabatic semiprognostic method can substantially improve simulations of oceanic biogeochemical cycles in a computationally efficient and conceptually appealing way. To quantify the impact of the semiprognostic correction to the circulation and the implied carbon uptake by the North Atlantic we compare the model bias of the uncorrected model version with sensitivity experiments that represent present uncertainties in the formulation of the air-sea gas exchange.

[7] The paper is organized as follows: In the following section we present the configuration of the biogeochemical model which is, as in OCMIP-2, identical in all model experiments. The different physical configurations of the model are described in section 3, and model results are presented and discussed in section 4. The last section summarizes and discusses our conclusions. Several important model-specific details are included in Appendix A.

2. Biogeochemical Model Configuration

[8] A pelagic ecosystem model (NPZD) is coupled to a number of different physical configurations of a regional ocean general circulation model (OGCM) of the North Atlantic. The nitrogen-based NPZD model consists of four compartments: nutrients, phytoplankton, zooplankton and detritus, interacting with each other as described by *Oschlies and Garçon* [1999]. The biological source and sink terms exactly conserve nitrogen, but the presence of open boundaries and restoring zones compromises total nitrogen conservation in the regional model. All parameters of the NPZD model are the same as in the work of *Oschlies and Garçon* [1999]. In particular, detritus is the only compartment that moves relative to the water with a constant sinking velocity of 5 m/day. The model does not have a sediment module, and all organic matter reaching the bottom remains in the deepest grid box where it is subject to advection, mixing, and remineralization (as in the free water column). Corresponding to the OCMIP guidelines, dissolved inorganic carbon (DIC) and dissolved oxygen are coupled to the nitrogen-based ecosystem model via the standard Redfield ratio for C:N (6.625 mol C/mol N) and an updated ratio for O_2:N (-10.0 mol O_2/mol N). Denitrification is not included in the model. To avoid oxygen becoming negative below highly productive areas, oxygen utilization is stopped in the model once oxygen concentrations reach zero (remineralization of organic nitrogen and carbon back to the respective inorganic compartments does, however, continue). In contrast to the compartments of the NPZD model, the distributions of DIC and oxygen are also affected by air-sea fluxes, which are discussed below.

[9] The physical models are integrated in each configuration from rest in a decadal scale spin-up integration to allow for a quasisteady dynamical equilibrium. After this spin-up period, the biogeochemical tracers are added and the coupled models are then integrated for further 50 years. Initial conditions for nitrate and oxygen are taken from *Boyer and Levitus* [1997], for DIC from the observational estimate of preindustrial DIC from GLODAP [*Sabine et al.*, 2004]. Initial conditions for phytoplankton, zooplankton and detritus are set to small values [*Oschlies and Garçon*, 1999]. Lateral boundary conditions are needed at the open boundary conditions [*Stevens*, 1990] at 20°S and 70°N and for a restoring zone (which has the same extent and damping timescale as for temperature and salinity) in the Gulf of Cadiz since the Mediterranean Sea is not part of the model domain. All lateral boundary conditions are taken from the initial conditions. We have also implemented restoring zones (with a 3-day restoring timescale) for nitrate, DIC, and oxygen over a 10-grid-point distance from the northern and southern open boundary conditions to keep inflow and outflow of the respective tracers close to observations in case of physical model biases near the open boundaries. (Note that open boundaries, although clearly a better alternative than buffer zones, will never work perfectly. Therefore model biases in the circulation are likely to show up here.)

[10] The surface boundary conditions for DIC and oxygen are calculated following the OCMIP standards: The air-sea difference in partial pressure of CO_2 (ΔpCO_2) is calculated from total alkalinity, DIC, temperature, salinity and atmospheric total sea level pressure (SLP) by solving iteratively for the roots of a high order polynomial equation for the total concentration of the H^+ ions (pH) using the code

provided by OCMIP. Contributions by variable nitrate, silicate, phosphate, etc., concentrations on pH are neglected. Since alkalinity is not a prognostic model variable, we use a nonlinear empirical fit of surface alkalinity versus sea surface salinity based on observations from the North Atlantic (see Appendix A). SLP strongly influences ΔpCO_2 and therefore we use a seasonally and spatially varying SLP climatology for the ΔpCO_2 formulation in the model taken from the NCEP/NCAR reanalysis data [*Kalnay et al.*, 1996]. The atmospheric partial pressure of CO_2 remains at a preindustrial level, but varies seasonally and latitudinally according to a nonlinear fit to observational estimates by *Conway et al.* [1994] as described in Appendix A. Sensitivity experiments revealed that the use of seasonally and spatially variable SLP and atmospheric partial pressure of CO_2 in the ΔpCO_2 formulation can change the carbon uptake of the Atlantic locally by 10% (not shown, however). Another potentially important aspect is the choice of the piston velocities for the parameterization of the turbulent air-sea fluxes of carbon and oxygen. Here we use the formulation of *Wanninkhof* [1992] for monthly mean wind speed data taken from the NCEP/NCAR reanalysis, except for one model experiment explained below.

3. Physical Model Configuration

[11] The NPZD model is embedded into a regional OGCM based on the FLAME (http://www.ifm.uni-kiel.de/fb/fb1/tm/research/FLAME/index.html) hierarchy of North Atlantic models at different horizontal resolutions (4/3°, 1/3° and 1/12°) based on a rewritten version of MOM2 [*Pacanowski*, 1995] (the numerical code together with all configurations used in this study can be accessed at http://www.ifm.uni-kiel.de/fb/fb1/tm/data/pers/ceden/spflame/index.html). These models have been analyzed and discussed with respect to various aspects of their mean state and seasonal and interannual variability by, for example, *Eden and Jung* [2001] and *Eden and Böning* [2002], where various model details can be found as well. Here we focus on the eddy-permitting (1/3°) version of the model in different configurations. All configurations share the same model domain, spanning the Atlantic Ocean from 20°S to 70°N at horizontal resolution of $1/3° \times 1/3° \cos\phi$ (ϕ denoting latitude) and 45 vertical levels (ranging from 10 m thickness near the surface to 250 m below approximately 2000 m). We discuss three model experiments (experiments BIHARM, PROG and SEMI) that differ only in the physical model configuration, and one sensitivity experiment that utilizes a different air-sea carbon flux formulation (experiment WIND). The pelagic ecosystem model and all forcing functions are identical in all experiments. All experiments employ the Multidimensional Positive Definite Central Differences (MPDCD) method proposed by *Lafore et al.* [1998] for the biogeochemical tracers to prevent the generation of negative tracer concentrations by spurious undershooting, an inherent artifact of dispersive advection schemes like standard central differencing.

3.1. Experiment BIHARM

[12] The BIHARM configuration is very similar to the z-level model which was part of the European "DYNAMO" ocean model intercomparison project [*Willebrand et al.*, 2001]. In particular, it uses the same horizontal resolution, the same surface boundary forcing (i.e., monthly mean wind stress, Haney-type heat flux condition as given by *Barnier et al.* [1995], and a restoring condition for sea surface salinity) and the same lateral boundary conditions along 20°S and in the Gulf of Cadiz as in DYNAMO. North of the Greenland-Iceland-Scotland ridge system, however, an open boundary condition at 70°N replaces a buoyancy restoring zone to account for a more realistic inflow (outflow) of arctic (subpolar) water masses across the ridge system [*Czeschel*, 2005]. (The prescribed data for the barotropic inflow were made available by the Arctic Modeling Group at AWI Bremerhaven, Germany (R. Gerdes, personal communication, 2004).) Another difference in the present setup to DYNAMO is the increased vertical resolution (45 levels) and therefore newly interpolated topography and a different closure for vertical diffusion and viscosity following *Gaspar et al.* [1990], utilizing identical parameters as *Oschlies and Garçon* [1999]. This scheme is used in all model experiments.

3.2. Experiment PROG

[13] The configuration of experiment PROG is identical to BIHARM with the following exception: since the horizontal resolution of the model is too coarse to adequately resolve mesoscale activity over large regions of the model domain, we use an eddy parameterization in these regions. The regions are identified by comparing the local grid resolution with the internal Rossby radius as a measure of the scale that has to be resolved to allow for mesoscale activity. Whenever the local grid spacing is smaller than the internal Rossby radius, we assume that eddies are resolved and apply similar subgridscale damping schemes as in experiment BIHARM. (In contrast to BIHARM, however, biharmonic diffusion is not used in "eddy-resolving regions" in PROG. Here we use the Quicker advection scheme [*Leonard*, 1979] in the entire model domain instead of the simple second-order centered differences scheme used in DYNAMO and BIHARM. Note that Quicker contains (small) implicit diffusion such that we use Quicker without additional explicit diffusion which appears to be sufficient to damp grid-scale noise. We also do not apply additional (lateral) damping to tracers when using isopycnal diffusion. Identical biharmonic viscosity, however, is used in all model cases.) Whenever the local horizontal grid resolution is coarser than the local Rossby radius, we apply isopycnal harmonic diffusion [*Redi*, 1982] to parameterize mixing by eddies and isopycnal thickness diffusion [*Gent and McWilliams*, 1990] to parameterize advective effects by eddies. A smooth transition is applied between the two regions. The scheme is explained in more detail in Appendix A.

[14] We use the above described method as an objective way to decide which regions are adequately resolved such that we can expect to realistically simulate the vigorous eddy activity and in which regions we have to parameterize the eddy effect. Basically, the latter regions are north of about 40°N and in shallow regions along the continental shelves (not shown). Note that in the "eddy-resolving

regions'', i.e., the interior Atlantic south of 40°N, we can expect experiment PROG to behave similar to BIHARM. Note also that we are not proposing the above described method as a ''new eddy parameterization''; it just results from the problem that the (eddy-permitting) model grid only partly resolves mesoscale activity. The aim of experiment PROG is to test whether an eddy parameterization applied in ''non-eddy-resolving regions'' can significantly improve the simulation of an eddy-permitting model.

3.3. Experiment SEMI

[15] The configuration of experiment SEMI is identical to that of PROG, but applies the semiprognostic method proposed by *Sheng et al.* [2001] and *Eden et al.* [2004]. In this simple data assimilative approach to adjust the flow field of the model, the dynamically active in situ density (ρ^*) that forces the horizontal momentum equation via the horizontal pressure gradient is given as a linear combination of an a priori known density (ρ_c) and the density calculated from the model's actual temperature and salinity (ρ_m), i.e., as

$$\rho^* = \alpha\rho_m + (1-\alpha)\rho_c, \tag{1}$$

where ρ^* is used during the model integration to calculate the ''baroclinic part'' of the horizontal pressure gradient in the horizontal momentum equation obtained by vertically integrating the hydrostatic equation. (There is also a part of the pressure gradient resulting from the sea surface elevation or surface pressure (in case of a rigid lid) which is left unchanged.) No changes are applied to the temperature, salinity, or any other tracer equation; all changes are confined to the horizontal pressure gradient in the horizontal momentum equation only. Of course, changes in the momentum equation will, via changes in the advective velocities, indirectly affect temperature, salinity and the biogeochemical tracers as well. For simplicity, the parameter α is set to 0.5, but see *Sheng et al.* [2001] for a more detailed discussion of α. To calculate ρ_c, we use the climatology of temperature and salinity given by *Boyer and Levitus* [1997] serving also as initial and lateral boundary condition for the model. However, as demonstrated by *Eden et al.* [2004], it turns out that rewriting the above equation as

$$\rho^* = \rho_m + (1-\alpha)(\rho_c - \rho_m) \tag{2}$$

and averaging the second (correction) term on the r.h.s (in time over 1 year and space over 5 grid points) successfully removes drawbacks of the original method: damped mesoscale activity and spurious interaction with topography. Furthermore, it is possible to diagnose the correction term in a spin-up integration and use it as a fixed correction for the sum of effects of unresolved processes and model biases in a subsequent integration. Then another drawback of the original method, namely reduced geostrophic wave speeds, is removed. While we do not apply this last step in the current study, we expect no large effects on the results presented here [*Eden et al.*, 2004]. Note that there is no guarantee for convergence of the method, as discussed by *Eden et al.* [2004] and *Greatbatch et al.* [2004]. More details and discussion of the semiprognostic method are given in a review article by *Greatbatch et al.* [2004].

[16] Again, we want to stress that since the semiprognostic method affects the momentum equation only, it is well suited for the simulation of passive tracers in contrast to other simple data assimilation schemes. It has been shown by *Sheng et al.* [2001] and *Eden et al.* [2004] that the method can significantly improve flow characteristics and water mass properties of eddy-permitting models of the North Atlantic. Therefore we expect a similar improvement in the simulation of carbon uptake of the North Atlantic, which we shall indeed demonstrate below. Note, however, that because of its need for climatological density data ρ_c in the correction term (although ρ_c can, in principle, vary with time), the method is not designed to simulate large deviations from present climate (in terms of density), i.e., in a drastic global warming scenario or in paleo climate simulations. Nevertheless, we expect that for small deviations from present climate, for instance hindcast simulations of the last 200 years, the configuration with fixed climatological density data employed here can account for model biases and is able to improve the simulation.

3.4. Experiment WIND

[17] The configuration of experiment WIND is identical to that of SEMI except for the formulation of the piston velocity for the air-sea carbon flux. Experiment WIND employs the formulation proposed by *Wanninkhof and McGillis* [1999] instead of *Wanninkhof* [1992] as used in the other experiments. Differences between these runs are deemed to reveal the influence of present uncertainties of turbulent surface flux parameterizations on CO_2 uptake of the North Atlantic. The piston velocity parameterization by *Wanninkhof* [1992] uses a quadratic relation to wind speed, while the one by *Wanninkhof and McGillis* [1999] uses a cubic function of wind speed. Because of the different dependence on wind speed the change to the *Wanninkhof and McGillis* [1999] formulation will lead to higher piston velocities in regions with large wind speeds, i.e., the subpolar North Atlantic, and lower piston velocities in regions with weaker wind speeds. Both formulations are given for the use with monthly mean wind speeds.

4. Results

[18] The following analysis concentrates on mid and high latitudes, since these regions are most important for the uptake of anthropogenic CO_2 [*Sabine et al.*, 2004]. Note, however, that the above introduced changes to the physical model component turn out to have rather little impact in the tropics and subtropics.

4.1. Influence of the Location of the Subpolar Front on Air-Sea CO_2 Fluxes

[19] Figure 1 shows the main difference in the near-surface water mass distribution in the experiments in terms of the near-surface temperature (at 20 m depth). This difference can be immediately related to the different paths of the Gulf Stream extension and North Atlantic Current

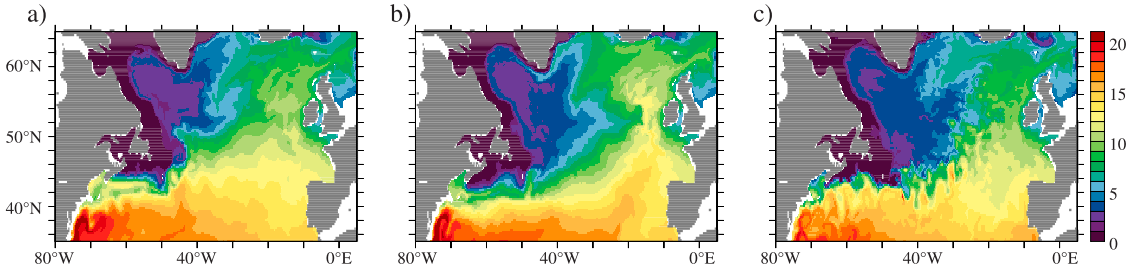

Figure 1. Snapshots of summertime potential temperature at 20 m depth in experiment (a) SEMI, (b) PROG, and (c) BIHARM in °C.

(NAC) off the coast of Newfoundland. In experiment SEMI, the NAC flows along the shelf break to the north and separates to the east from the shelf at about 50°N. In the experiments PROG and BIHARM, this so-called Northwest Corner of the NAC [*Lazier*, 1994] is missing, the NAC shows no northward turn and the flow is predominantly eastward. The effect of the different flow patterns is a northwestward shift of the western part of the subpolar front in SEMI compared to the other simulations. Since Figure 1 shows snapshots of the near-surface temperature, many mesoscale structures show up in the respective BIHARM figure along the subpolar front. These features are missing in the other two experiments which, at this latitude, parameterize the effect of the mesoscale eddies by an additional isopycnal thickness diffusivity in this region (since here the horizontal grid is coarser than the local Rossby radius). Note, however, that the mean position of the subpolar front and the general near-surface flow pattern and temperature distribution are similar in PROG and BIHARM. This indicates that these features are not significantly affected by the Rossby-radius dependent eddy parameterization employed in PROG (and SEMI).

[20] The results of experiment SEMI are closer to reality. This can be seen, for example, by looking at dissolved oxygen in the experiments. Figure 2 shows the mean near-surface oxygen distribution in SEMI, PROG and in observational estimates by *Boyer and Levitus* [1997]. The Gulf Stream and the NAC transport warm water masses with low oxygen concentrations to the north. In the observations a clear signature of low oxygen can be found off the coast of Newfoundland related to the path of the NAC. These low oxygen concentrations can also be found in the near-surface oxygen distribution in experiment SEMI while they are missing in experiment PROG that overestimates oxygen concentrations by up to 4 mL/L in this region. The near surface oxygen distribution in experiment BIHARM suffers from the same model bias and is therefore similar to that of experiment PROG and is not shown here.

[21] A similar signature of the subpolar front, given by the path of the NAC around the Grand Banks of Newfoundland can also be seen in the near-surface distribution of DIC. Figure 3 shows near-surface DIC concentrations of experiments SEMI, PROG, and BIHARM. In general, higher (lower) DIC concentrations are found north (south) of the subpolar front, associated with colder (warmer) subpolar (subtropical) waters. Similar to oxygen, a sharp lateral DIC gradient marks the location of the subpolar front in all experiments. Different locations of this front in the different experiments generate regional simulated DIC differences of up to 100 mmol/m^3 off the coast of Newfoundland.

[22] Another, although less prominent, difference in near-surface DIC can be noticed in the subpolar North Atlantic comparing the model experiments with and without the GM parameterization. There are in general higher DIC concentrations in BIHARM compared to PROG and SEMI, which is related to differences in the maximal wintertime mixed layer depth (MLD, not shown). In BIHARM, the MLD in the subpolar North Atlantic is larger compared to the experiments including the GM parameterization, i.e., PROG and SEMI. Since GM tends to flatten isopycnals, the effect of the parameterization is acting against steep isopycnal slopes near the surface during cooling in wintertime, leading

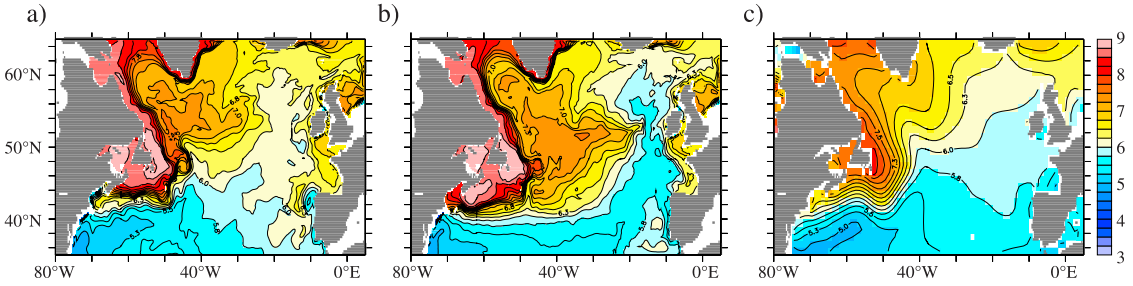

Figure 2. Three-year averages of near-surface dissolved oxygen (at 50 m) in experiments (a) SEMI and (b) PROG, and (c) observational estimates by *Boyer and Levitus* [1997] in mL/L.

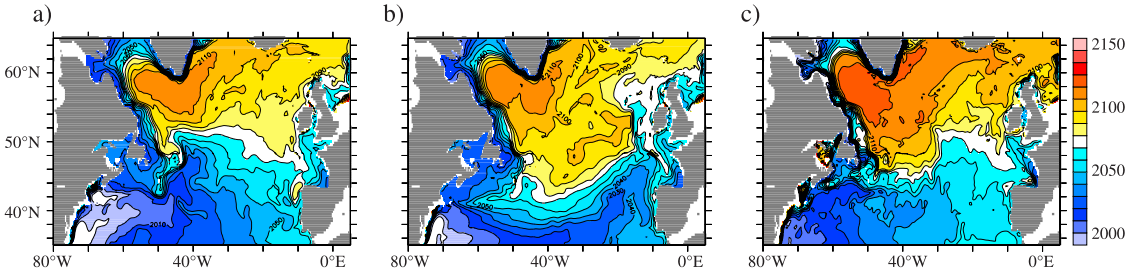

Figure 3. Three-year averages of near-surface dissolved inorganic carbon at 50 m depth in experiments (a) SEMI, (b) PROG, and (c) BIHARM in mmol/m^3.

to shallower MLD during winter in PROG and SEMI. Because of the deeper MLD in BIHARM, the higher DIC content of the mixed layer needs more time to equilibrate with the atmosphere. In the subpolar North Atlantic, there is continuous release of carbon during winter; thus DIC concentrations in the mixed layer will decrease (neglecting other effects as mixed layer deepening, advection or biological production and respiration). This decrease in surface DIC concentrations is smaller when the DIC content is larger in the deeper mixed layer; thus higher DIC concentrations are simulated in BIHARM during winter compared to PROG and SEMI.

[23] It is obvious that the dislocation of the subpolar front in the uncorrected model will have an impact on the simulated air-sea CO_2 fluxes. Figure 4 shows CO_2 fluxes in experiment SEMI and PROG, together with observational estimates by *Takahashi et al.* [2002] (we have obtained these data from http://www.ldeo.columbia.edu/res/pi/CO2/carbondioxide/air_sea_flux/fluxdata.txt, which represent a corrected version of the original publication because the fluxes are now calculated with 10-m wind speeds for the piston velocities). The figure shows that in experiment PROG, the bias in near-surface temperature and DIC concentration off the coast of Newfoundland leads to release of CO_2 in this region. In contrast, experiment SEMI simulates CO_2 uptake in large regions of the subpolar North Atlantic and only a small region of CO_2 release in the Gulf Stream separation region. This is in better agreement with the observational estimates by *Takahashi et al.* [2002] that indicate an uptake of CO_2 over the entire subpolar North Atlantic. Note, however, that a direct comparison of the observed present-day CO_2 fluxes with our preindustrial simulations is difficult. On the other hand, for the simulation in PROG to be valid we would at least expect a local minimum in CO_2 uptake by the ocean off the coast of Newfoundland in the observations. Instead, these show a local CO_2 uptake maximum in this region.

4.2. Interaction of Physical and Biological Effects at the Subpolar Front

[24] Since the piston velocity depends only weakly on changes in surface temperature (only by 2–3% per Kelvin), the difference in the air-sea CO_2 fluxes between experiment SEMI and PROG are predominantly given by differences in surface pCO_2, Figure 5a shows the difference in surface pCO_2 between SEMI and PROG. A large negative anomaly up to about −100 ppm shows up along the subpolar front. Surface pCO_2 in our model setup is a function of salinity, temperature and DIC only. Therefore we can partition the total pCO_2 difference between experiments SEMI and PROG to contributions from changes in surface salinity, temperature and DIC according to

$$\Delta pCO_2 = \frac{\partial pCO_2}{\partial S}\Delta S + \frac{\partial pCO_2}{\partial T}\Delta T + \frac{\partial pCO_2}{\partial DIC}\Delta DIC + o\left(\Delta^2\right), \tag{3}$$

where ΔpCO_2, ΔS, ΔT and ΔDIC denote the difference (perturbation) of pCO_2, surface salinity, temperature and

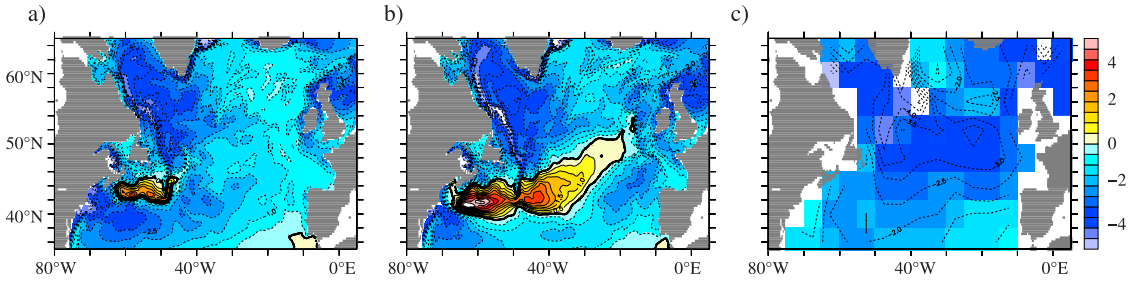

Figure 4. Three-year averages of air-sea CO_2 fluxes in experiment (a) SEMI and (b) PROG and (c) in observational estimates by *Takahashi et al.* [2002] in mol/m^2/yr. Negative values denote uptake of CO_2 by the ocean.

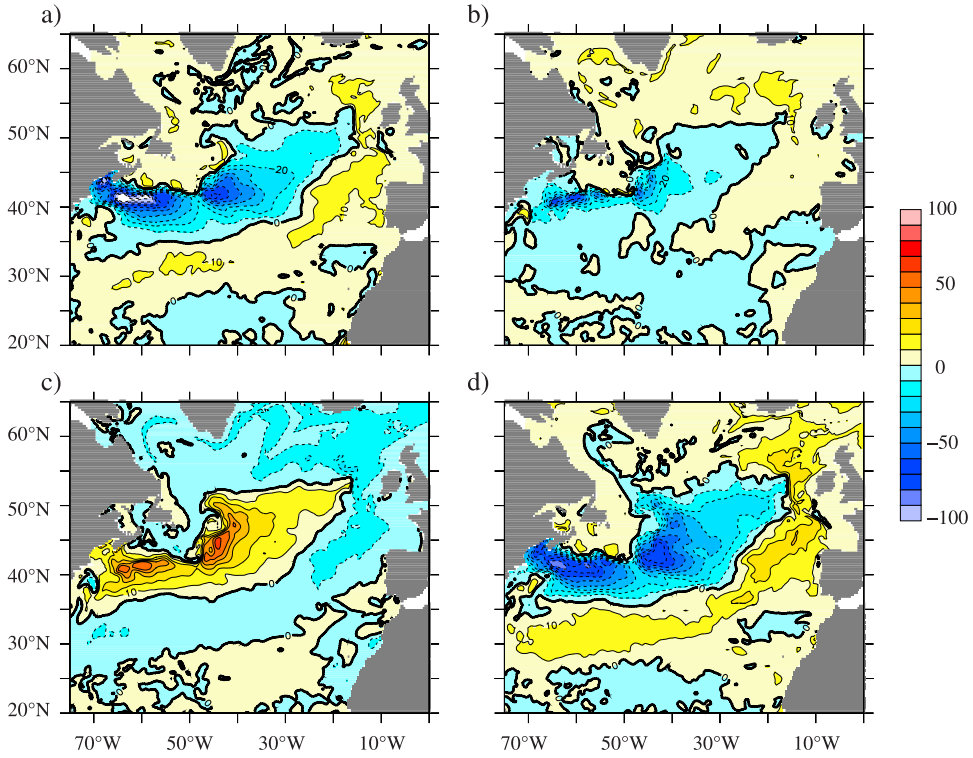

Figure 5. (a) Difference in sea surface pCO_2 between experiment SEMI and PROG (SEMI-PROG) in ppm. (b) Difference due to change in salinity, $\frac{\partial pCO_2}{\partial S}\Delta S$. (c) Difference due to change in temperature, $\frac{\partial pCO_2}{\partial T}\Delta T$. (d) Difference due to change in DIC, $\frac{\partial pCO_2}{\partial DIC}\Delta DIC$.

DIC between both experiments respectively (SEMI-PROG) and $o(\Delta^2)$ terms of second (and higher) order in perturbation quantities. The partial derivatives $\frac{\partial pCO_2}{\partial S}$, $\frac{\partial pCO_2}{\partial T}$ and $\frac{\partial pCO_2}{\partial DIC}$ are functions of salinity, temperature and DIC as well and are derived from a third-order polynomial fit of pCO_2 (given by the OCMIP routine) as a function of salinity, temperature and DIC. Typical values of the partial derivatives are about $\frac{\partial pCO_2}{\partial T} \approx 10$, ppm/K and $\frac{\partial pCO_2}{\partial DIC} \approx 1$ ppm/mmol m^{-3}. Since alkalinity is a function of salinity in our model setup, $\frac{\partial pCO_2}{\partial S}$ can be decomposed into two parts,

$$\frac{\partial pCO_2}{\partial S} = \left.\frac{\partial pCO_2}{\partial S}\right|_{Alk=const} + \left.\frac{\partial pCO_2}{\partial Alk}\right|_{S=const} \frac{\partial Alk}{\partial S}, \qquad (4)$$

of which the latter term dominates such that a mean value is given by $\frac{\partial pCO_2}{\partial S} \approx \frac{\partial pCO_2}{\partial Alk}\frac{\partial Alk}{\partial S} \approx -60$ ppm/psu. Note that the second order terms in equation (3) ($o(\Delta^2)$) contribute more than 1 order of magnitude less than the first-order terms and are neglected in the following.

[25] Figures 5b, 5c and 5d show the three individual contributions to the total pCO_2 change. The pCO_2 changes due to differences in DIC and temperature between SEMI and PROG clearly dominate the pCO_2 change due to the difference in salinity. Since off the coast of Newfoundland the difference in surface temperature between SEMI and PROG (SEMI-PROG) is positive, the pCO_2 change due to the temperature change is positive. On the other hand, the difference in surface DIC is negative in this region, which yields a negative pCO_2 change. Both contributions nearly cancel, such that the smaller contribution by the change in salinity also plays a role. The northwestward shift in the subpolar front in SEMI compared to PROG also leads to a positive surface salinity anomaly (not shown), since surface subtropical waters are more saline than those of the subpolar North Atlantic. Because of the negative impact of salinity changes on pCO_2, the salinity change generates a negative pCO_2 change in SEMI. Note that the direct impact of the salinity change on pCO_2 is negligible. It is its indirect effect via alkalinity which leads to the pCO_2 changes. For a better indication of the magnitudes of the different terms playing a role in setting pCO_2 in the subpolar North Atlantic and the region off the coast of Newfoundland, Figure 6 shows the total pCO_2 change and its three individual contributions to the total change along 40°W.

[26] Changes in DIC and related changes in pCO_2 can be generated by changes in surface advection in the different experiments, but also by local changes in biological production. To show the net contribution by the simulated biological production, we have averaged the source term in the carbon budget due to biological activity (e.g., primary production minus remineralization) in time over 3 years after the spin-up of the model. The source term is predominantly positive (net nutrient consumption) in the euphotic zone and negative below (net remineralization). This source term is sometimes called "net community production" (see also a discussion of the various definitions of the biological production by *Oschlies and Kähler* [2004]). It is integrated

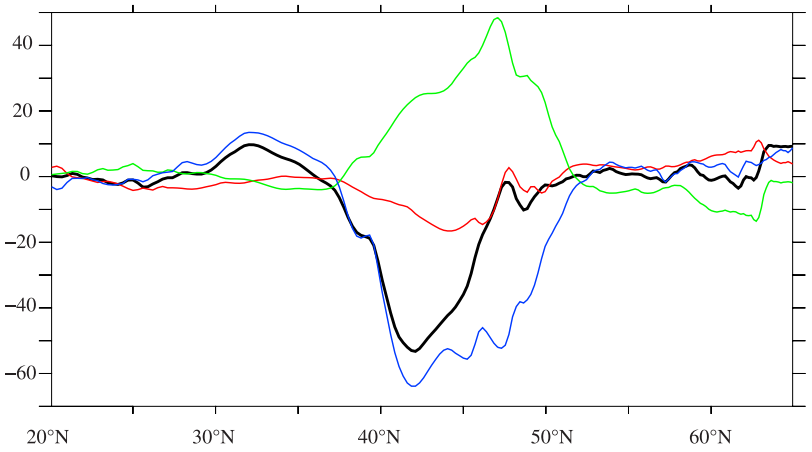

Figure 6. Difference in sea surface pCO_2 at 40°W between experiment SEMI and PROG (SEMI-PROG) in ppm (black line). Difference due to change in salinity, $\frac{\partial pCO_2}{\partial S}\Delta S$ (red line). Difference due to change in temperature, $\frac{\partial pCO_2}{\partial T}\Delta T$ (green line). Difference due to change in DIC, $\frac{\partial pCO_2}{\partial DIC}\Delta DIC$ (blue line).

over the annual cycle and the maximal mixed layer depth reached during 3 years after the spin-up and shown in Figure 7 for SEMI and PROG in terms of a downward carbon flux. The magnitude of this flux is of the same order as the surface carbon flux, and similar to the results obtained for a different model by *Oschlies and Kähler* [2004, Figure 8d] with differences being related mainly to differences in the simulated mixed layer depth. It is more difficult to compare this flux with other studies that often show quantities related to the carbon drawdown from the euphotic zone, but with a different meaning as the one diagnosed in this study (see discussion by *Oschlies and Kähler* [2004]). However, at least we can note that magnitude and pattern in Figure 7 are similar to, for example, the equivalent carbon flux by new production from the euphotic zone in the model of *McGillicuddy et al.* [2003, Figure 6a], although mesoscale variability interacting with the subsurface nitrate restoring applied in the model of *McGillicuddy et al.* [2003] complicate the interpretation of their results and comparison with the present results.

[27] Figure 7 reveals that the northwestward shift of the subpolar front in experiment SEMI reduces the simulated downward flux of carbon due to the biological pump in the subpolar North Atlantic. The lowered downward flux will tend to increase surface DIC and pCO_2 in SEMI compared to PROG and will therefore tend to reduce the carbon uptake of the subpolar North Atlantic in SEMI. Integrating the downward export of carbon across the maximal mixed layer depth over the region shown in Figure 7 yields 30×10^{12} mol/yr for experiment SEMI and 38.5×10^{12} mol/yr for PROG. Note that for a similar physical and biogeochemical model, *Oschlies and Kähler* [2004] obtain a value of 23.2×10^{12} mol/yr for the same region. Neglecting effects due to changes in the subduction or entrainment of biotically generated carbon anomalies, the difference between SEMI and PROG corresponds to a 25% decrease of biotically effected carbon drawdown in SEMI. On the other hand, the total uptake of CO_2 in experiment SEMI for the region shown in Figure 4 is 22.37×10^{12} mol/yr and 16.55×10^{12} mol/yr for PROG, thus about 25% more uptake

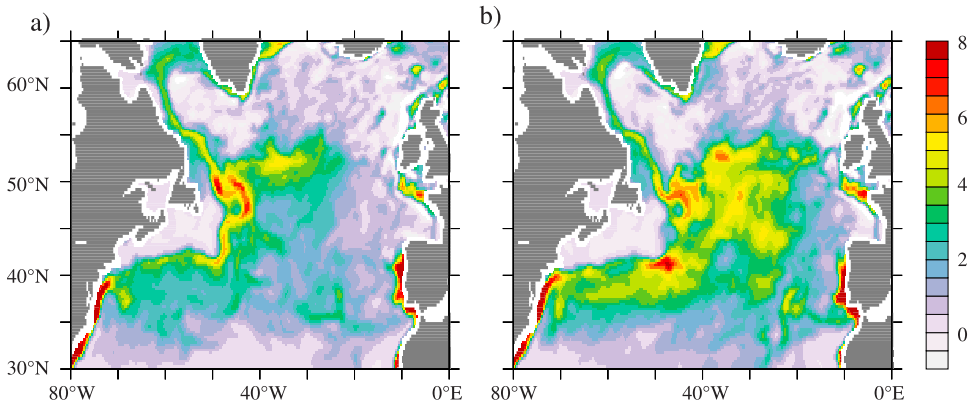

Figure 7. Annual net community production integrated over the maximal mixed layer depth reached during 3 years after the spin-up in (a) SEMI and (b) PROG in mol/m^2/yr carbon.

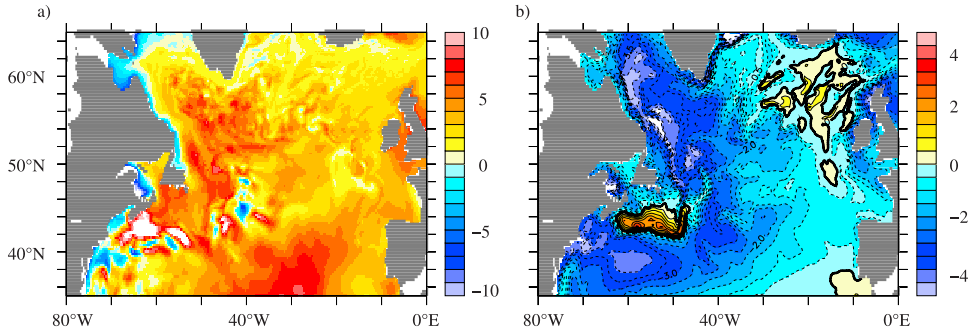

Figure 8. (a) Difference in sea surface pCO_2 between experiment WIND and SEMI (WIND-SEMI) in ppm. (b) Air-sea CO_2 flux in experiment WIND in mol/m^2/yr.

in the corrected model version. Note that the decreased biological carbon drawdown in SEMI acts opposite to the overall increase in carbon uptake in this experiment.

4.3. Influence of Parameterizations of Air-Sea Gas Exchange

[28] An often acknowledged uncertainty in simulated air-sea CO_2 fluxes is caused by uncertainties in the parameterization of air-sea gas exchange [*England et al.*, 1994; *Beismann and Redler*, 2003]. To test this influence in our model setup, we have changed the piston velocity parameterization in experiment WIND from the formulation by *Wanninkhof* [1992] which uses a quadratic relation to wind speed to the one by *Wanninkhof and McGillis* [1999] which uses a cubic function of wind speed. This change will lead to higher piston velocities in regions with large wind speeds, like the subpolar North Atlantic, and lower piston velocities in regions with weaker wind speeds. Using observational estimates of air-sea pCO_2 differences, *Wanninkhof and McGillis* [1999] find that using the cubic relation leads to an increase in global oceanic CO_2 uptake by more than 50% compared to the quadratic relation to wind speed.

[29] The effect in our model setup is shown in Figure 8. Surface pCO_2 values are indeed higher by about 5 ppm in experiment WIND compared to SEMI in the subpolar North Atlantic. These higher values are generated by stronger CO_2 uptake in WIND. Figure 8b shows the air-sea CO_2 fluxes in WIND on the same color scale as for the other experiments (Figure 4). Note that changes in pCO_2 are entirely given by changes in DIC on the order of 5 mmol/m^3. The total CO_2 uptake for the region shown in Figure 8b in WIND is 25.35×10^{12} mol/yr, thus about 10% larger compared to experiment SEMI.

5. Conclusions and Discussion

[30] We have demonstrated that incorrect flow pathways in ocean models, identified in this study as a missing Northwest Corner of the NAC [*Lazier*, 1994] and a dislocated subpolar front as prominent and well-known example of a serious bias in models of the North Atlantic [*Willebrand et al.*, 2001], can lead to changes in total CO_2 uptake of as much as 25% in our model setup. By correcting the simulated circulation using the adiabatic semiprognostic method, we were able to improve this model bias and to quantify its impact on CO_2 uptake. The impact of this correction is large compared to typical uncertainties in the parameterization of air-sea gas exchange. Note that in contrast to robust-diagnostic restoring techniques used previously in order to avoid models drifting too far away from the observations [*Aumont et al.*, 1999; *LeQuere et al.*, 2000], our adiabatic semiprognostic method exactly conserves water mass properties and tracers everywhere. The correction term perturbs the momentum equations only, whereas all tracers still evolve in a dynamically consistent manner. Of course, changes in the momentum equation will indirectly affect temperature, salinity and the biogeochemical tracers as well by changes in the advective velocities.

[31] In the uncorrected model versions, the missing Northwest Corner of the NAC manifests itself in a southeastward shift of the western part of the subpolar front that exhibits one of the largest gradients in near-surface temperature, salinity, DIC, biomass, nutrients and oxygen in the North Atlantic. The corrected model yields a more realistic advection of warm subtropical waters into the area of the Northwest Corner off Newfoundland, which increases surface pCO_2. On the other hand, these waters also have relatively low DIC and nutrient concentrations. The advection of water low in DIC decreases surface pCO_2, while the decreased biological export production coming along with the reduced advection of nutrients leads to a reduced drawdown of near-surface DIC and to an increase in surface pCO_2. A smaller contribution comes from a decrease in pCO_2 due to advection of water high in alkalinity. The interaction of the strong (and opposing) pCO_2 controls by near-surface temperature, DIC concentrations and biological activity on pCO_2 together with the small contribution by alkalinity in this region essentially determines the CO_2 uptake by the subpolar North Atlantic. With respect to the differences between corrected and uncorrected model runs, the controls acting to decrease pCO_2 (lower DIC by advection, higher Alkalinity) have a larger impact than the controls acting to increase pCO_2 (higher SST, higher DIC by less net community production). We speculate that the effect of the model bias on the carbon uptake would be even larger without the damping influence of the reduced drawdown of carbon by the biological pump, which decreases by 25% in the subpolar North Atlantic in the corrected-physics run.

[32] The close cancellation of DIC and SST controls on pCO_2 and the resulting importance of advection of alkalinity

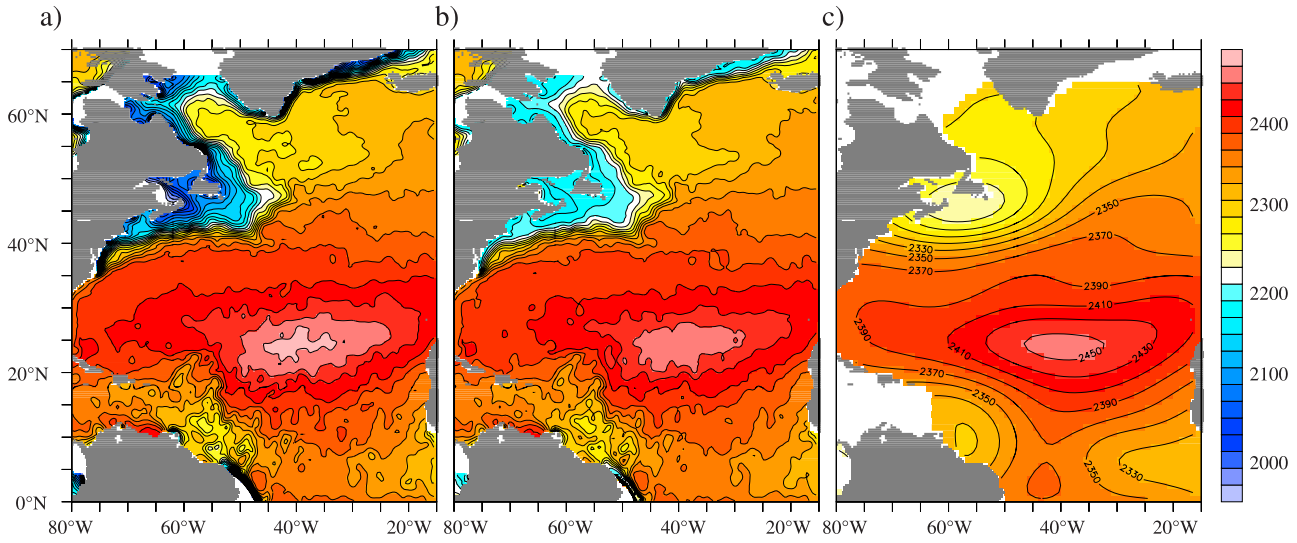

Figure A1. Sea surface alkalinity in mmol/m^3 from (a) the linear fit versus against salinity given by the (abiotic) OCMIP protocol, (b) the nonlinear fit used in this study, and (c) an observational estimate of alkalinity from the GLODAP gridded data set.

raises the question of how much the parameterization of alkalinity as a function of salinity influences the results presented here. Note that we use a functional form which, for the North Atlantic, is in better agreement to observational estimates than the simple linear relationship on salinity used in the abiotic simulations of OCMIP (see Appendix A). While it is certainly desirable to include alkalinity as a prognostic variable, the currently poor knowledge about formation and dissolution of calcium carbonate makes this still a challenging task. Further model improvements as, for example, the explicit representation of dissolved organic carbon may also influence the simulated CO_2 uptake in the North Atlantic. We nevertheless expect that biases in the upper ocean circulation, such as shown above, have a dominant impact on the simulated CO_2 uptake.

[33] The conclusions derived here for a simulation of the preindustrial carbon cycle will also apply for simulations of anthropogenic CO_2 uptake of which a large fraction takes place in the subpolar North Atlantic [*Sabine et al.*, 2004]. On the basis of our model results and having in mind the large variety of model solutions in OCMIP, we think that it must be a priority to simulate the circulation and physical environment correctly, before attempting to improve the biogeochemical model. For the North Atlantic, we have demonstrated that this is possible using the semiprognostic method in a computationally efficient way.

Appendix A

A1. Alkalinity as a Function of Salinity

[34] Since alkalinity is not a prognostic model variable, we use a nonlinear empirical fit of surface alkalinity versus sea surface salinity based on observational estimates for the North Atlantic domain. This fit is given by

$$Alk = -0.5487S^3 + 59.919S^2 - 2122.3S + 26722, \qquad \text{(A1)}$$

where Alk is alkalinity in mmol/m^3 and S salinity in psu. Note that this fit deviates from the (linear) fit proposed for abiotic simulations in the OCMIP protocol. The fitted alkalinity is shown in Figure A1 using sea surface salinity from *Boyer and Levitus* [1997], which is also used in the model for the restoring of sea surface salinity. Figure A1a shows alkalinity for the fit from the OCMIP protocol, Figure A1b for the fit used in our model experiments and Figure A1c sea surface alkalinity from the GLODAP gridded data set for comparison.

[35] Over wide regions in the subtropical North Atlantic there are no large differences between both fits and the observational estimate. Approaching the coast of North America, both fits give lower alkalinities than the observations, lowest values are given by the linear fit around Newfoundland. Note that the error estimate (due to the interpolation scheme) given by GLODAP is highest in this region as well, around 30 mmol/m^3. However, the linear fit deviates from GLODAP by more than 100 mmol/m^3 in this region, compared to the about 50 mmol/m^3 deviation of the nonlinear fit. Note that a bias of 50 mmol/m^3 would result in a 50 ppm bias in sea surface pCO_2, leading to a large bias in the air-sea carbon flux.

A2. Latitudinal and Seasonal Dependency of Atmospheric Partial Pressure of CO_2

[36] The atmospheric partial pressure of CO_2 used in the model integration remains on a preindustrial level, but it varies with season and latitude following a nonlinear fit to observational estimates by *Conway et al.* [1994], as shown in Figure A2. The fit is given by

$$\begin{aligned} pCO_2 = {} & 279.2472 + 0.0353y + 3.3458 \times 10^{-5}y^2 - 2.6829 \\ & \times 10^{-6}y^3 + [0.9626\sin(2\pi t - 0.1349) - 0.2708\sin(4\pi t \\ & - 0.5242)] \times \left[1.3971 + 7.6558\left(1 + \tanh\frac{y - 24.7554}{26.5702}\right)\right], \end{aligned} \qquad \text{(A2)}$$

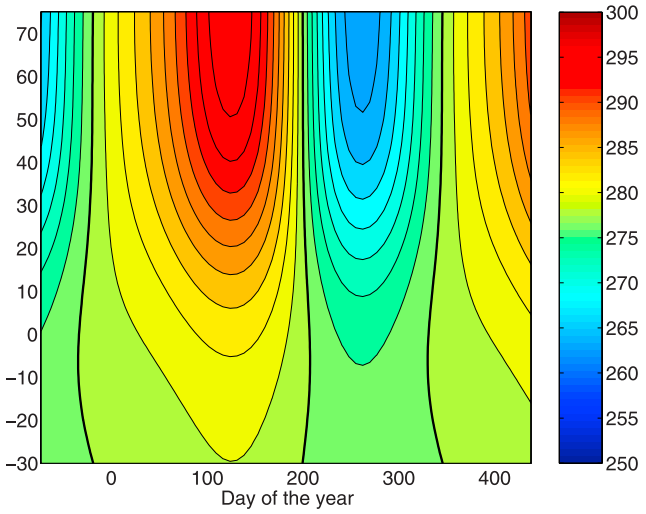

Figure A2. Atmospheric pCO_2 fit in ppm as a function of latitude and time. The solid line denotes the mean preindustrial value of 278 ppm.

where pCO_2 denotes atmospheric partial pressure in ppm, y latitude in degrees and t days of the current year divided by 365, i.e., $0 < t < 1$.

A3. Eddy Parameterization as a Function of the Local Rossby Radius

[37] Since the horizontal resolution of the eddy-permitting model is too coarse to adequately resolve mesoscale activity over large regions of the model domain, we use an eddy parameterization in these regions in experiments PROG, SEMI and WIND. This is done by comparing the local grid resolution with the internal Rossby radius as a rough measure of the scale which has to be resolved to allow for mesoscale activity. We calculate the first internal Rossby radius L_i as

$$L_i = \min\left[\frac{c_i}{|f|}\,,\ \sqrt{\frac{c_i}{2\beta}}\right], \tag{A3}$$

where c_i denotes the first baroclinic Rossby wave speed, f is the Coriolis parameter and $\beta = \frac{\partial f}{\partial y}$. The Rossby wave speed c_i is approximated at each model time step following *Chelton et al.* [1998] by $c_i \approx \int_{-h}^{0} N/\pi dz$, where N is the local stability frequency and h is the local water depth.

[38] We use isopycnal diffusion [*Redi*, 1982] to parameterize mixing by eddies and eddy-induced velocities [*Gent and McWilliams*, 1990] to parameterize advective effects by eddies with isopycnal (κ_{iso}) and thickness diffusivities (κ_{GM}) as a function of L_i (and depth). In case that the local horizontal grid resolution is coarser than L_i we use maximal values of 2×10^3 m^2/s for κ_{iso} and κ_{GM} and zero for both parameters otherwise. The functional dependence of κ_{iso} and κ_{GM} on L_i is given by

$$\Delta = \max[\Delta x \cos\phi\,,\ \Delta y] \tag{A4}$$

$$\kappa_{iso} = \kappa_{GM} = 2 \times 10^3 f(z)(1 - \tanh a_2(L_i/\Delta - a_1))/2\ \mathrm{m}^2/\mathrm{s}, \tag{A5}$$

where Δ_x and Δy denotes zonal and meridional grid resolution. The parameters a_1 and a_2 are set to 0.5 and 2, respectively. The functional form of $f(z)$ is the same as in the work of *Eden and Willebrand* [2001], i.e., at maximum one in the thermocline decaying to zero above and to 0.25 below. In addition, we use the third-order QUICKER advection scheme (based on the "quick" scheme of *Leonard* [1979], as implemented in MOM-3) in order to insure a stable integration in eddy-resolving regions where κ_{iso} and κ_{GM} are tapered to zero.

[39] **Acknowledgments.** This work was supported by the European Union within the project NOCES and, in part, by the Deutsche Forschungsgemeinschaft via the SFB 460. We thank two anonymous reviewers for their constructive comments.

References

Aumont, O., J. C. Orr, P. Monfray, G. Madec, and E. Maier-Reimer (1999), Nutrient trapping in the equatorial Pacific: The ocean circulation solution, *Global Biogeochem. Cycles*, *13*, 351–370.

Barnier, B., L. Siefridt, and P. Marchesiello (1995), Thermal forcing for a global ocean circulation model using a three year climatology of ECMWF analysis, *J. Mar. Syst.*, *6*, 363–380.

Beismann, J.-O., and R. Redler (2003), Model simulations of CFC uptake in North Atlantic Deep Water: Effects of parameterizations and grid resolution, *J. Geophys. Res.*, *108*(C5), 3159, doi:10.1029/2001JC001253.

Boyer, T. P., and S. Levitus (1997), Objective analyses of temperature and salinity for the world ocean on a 1/4 degree grid, *NOAA Atlas NESDIS 11*, Natl. Oceanic and Atmos. Admin., Silver Spring, Md.

Chassignet, E. P., and Z. D. Garraffo (2001), Viscosity parameterization and the gulf stream separation, in *From Stirring to Mixing in a Stratified Ocean*, edited by P. Müller and W. Henderson, pp. 37–41, Univ. of Hawaii at Manoa, Honolulu.

Chelton, D. B., R. A. deSzoeke, M. G. Schlax, K. E. Naggar, and N. Siwertz (1998), Geographical variability of the first-baroclinic rossby radius of deformation, *J. Phys. Oceanogr.*, *28*, 433–460.

Conway, T. J., P. P. Tans, L. S. Waterman, K. K. Thoning, D. R. Kitzis, K. A. Masarie, and N. Zhang (1994), Evidence for interannual variability of the carbon cycle from the National Oceanic and Atmospheric Administration/Climate Monitoring and Diagnostics Laboratory global air sampling network, *J. Geophys. Res.*, *99*(D11), 22,831–22,856.

Czeschel, L. (2005), The role of eddies for the formation of Labrador Sea water, Ph.D. thesis, Leibniz Institute for Marine Science at University of Kiel (IFM-GEOMAR), Kiel, Germany.

Doney, S. C., et al. (2004), Evaluating global ocean carbon models: The importance of realistic physics, *Global Biogeochem. Cycles*, *18*, GB3017, doi:10.1029/2003GB002150.

Eden, C., and C. W. Böning (2002), Sources of eddy kinetic energy in the Labrador Sea, *J. Phys. Oceanogr.*, *32*, 3346–3363.

Eden, C., and T. Jung (2001), North Atlantic interdecadal variability: Oceanic response to the North Atlantic oscillation (1865–1997), *J. Clim.*, *14*(5), 676–691.

Eden, C., and J. Willebrand (2001), Mechanism of interannual to decadal variability of the North Atlantic circulation, *J. Clim.*, *14*(10), 2266–2280.

Eden, C., R. J. Greatbatch, and C. W. Böning (2004), Adiabatically correcting an eddy-permitting North Atlantic model using large-scale hydrographic data: Application to the Gulf Stream and the North Atlantic Current, *J. Phys. Oceanogr.*, *34*, 701–719.

England, M. H., V. Garçon, and J. Minster (1994), Chlorofluorocarbon uptake in a world ocean model: 1. Sensitivity to the surface gas forcing, *J. Geophys. Res.*, *99*(C12), 25,215–25,234.

Ezer, T., and G. L. Mellor (1994), Diagnostic and prognostic calculations of the North Atlantic circulation and sea level using a sigma coordinate ocean model, *J. Geophys. Res.*, *99*(C7), 14,159–14,171.

Gaspar, P., Y. Gregoris, and J.-M. Lefevre (1990), A simple eddy kinetic energy model for simulations of the oceanic vertical mixing: Tests at station PAPA and Long-Term Upper Ocean Study site, *J. Geophys. Res.*, *95*(C9), 16,179–16,193.

Gent, P. R., and J. C. McWilliams (1990), Isopycnal mixing in ocean circulation models, *J. Phys. Oceanogr.*, *20*, 150–155.

Greatbatch, R. J., A. F. Fanning, A. D. Goulding, and S. Levitus (1991), A diagnosis of interpentadal circulation changes in the North Atlantic, *J. Geophys. Res.*, *96*(C12), 22,009–22,023.

Greatbatch, R., J. Sheng, C. Eden, L. Tang, X. Zhai, and J. Zhao (2004), The semi-prognostic method, *Cont. Shelf. Res.*, *24*(18), 2149–2165.

Kalnay, E., et al. (1996), The NCEP/NCAR 40-years reanalysis project, *Bull. Am. Meteorol. Soc.*, *77*, 437–471.

Lafore, J., et al. (1998), The Meso–NH atmospheric simulation system: Part 1. Adiabatic formulation and control simulations, *Ann. Geophys.*, *16*, 90–109.

Lazier, J. R. N. (1994), Observations in the Northwest Corner of the North Atlantic Current, *J. Phys. Oceanogr.*, *24*, 1449–1463.

Leonard, B. P. (1979), A stable and accurate convective modelling procedure based on quadratic upstream interpolation, *Comput. Methods Appl. Mech. Eng.*, *19*, 59–98.

LeQuere, C., J. C. Orr, P. Monfray, O. Aumont, and G. Madec (2000), Interannual variability of the oceanic sink of CO_2 from 1979 to 1997, *Global Biogeochem. Cycles*, *14*, 247–1265.

McGillicuddy, D. J., L. A. Anderson, S. C. Doney, and M. E. Maltrud (2003), Eddy-driven sources and sinks of nutrients in the upper ocean: Results from a 0.1° resolution model of the North Atlantic, *Global Biogeochem. Cycles*, *17*(2), 1035, doi:10.1029/2002GB001987.

Orr, J., et al. (2001), Estimates of anthropogenic carbon uptake from four three–dimensional global ocean models, *Global Biogeochem. Cycles*, *15*, 43–60.

Oschlies, A. (2002), Improved representation of upper-ocean dynamics and mixed layer depths in a model of the North Atlantic on switching from eddy-permitting to eddy-resolving grid resolution, *J. Phys. Oceanogr.*, *32*, 2277–2298.

Oschlies, A., and V. Garçon (1999), An eddy-permitting coupled physical-biological model of the North Atlantic: 1. Sensitivity to advection numerics and mixed layer physics, *Global Biogeochem. Cycles*, *13*, 135–160.

Oschlies, A., and P. Kähler (2004), Biotic contribution to air-sea fluxes of CO_2 and O_2 and its relation to new production, export production, and net community production, *Global Biogeochem. Cycles*, *18*, GB1015, doi:10.1029/2003GB002094.

Pacanowski, R. C. (1995), MOM 2 Documentation, User's Guide and Reference Manual, technical report, Ocean Group, Geophys. Fluid Dyn. Lab., Princeton, N. J.

Prentice, I. C., G. D. Farquhar, M. J. R. Fasham, M. L. Goulden, M. Heimann, V. J. Jaramillo, H. S. Kheshgi, C. Le Quere, R. J. Scholes, and D. W. R. Wallace (2001), The carbon cycle and atmospheric carbon dioxide, in *Climate Change 2001: The Scientific Basis. Contribution of Working Group I to the Third Assessment Report of the Intergovernmental Panel on Climate Change*, edited by J. T. Houghton et al., pp. 183–237, Cambridge Univ. Press, New York.

Redi, M. H. (1982), Oceanic isopycnal mixing by coordinate rotation, *J. Phys. Oceanogr.*, *12*, 1154–1158.

Sabine, C., et al. (2004), The oceanic sink for anthropogenic CO_2, *Science*, *305*(5682), 367–371.

Sarmiento, J. L., and K. Bryan (1982), An ocean transport model for the North Atlantic, *J. Geophys. Res.*, *87*(C1), 394–408.

Sheng, J., R. J. Greatbatch, and D. Wright (2001), Improving the utility of ocean circulation models through adjustment of the momentum balance, *J. Geophys. Res.*, *106*(C8), 16,711–16,728.

Smith, R. D., M. E. Maltrud, F. O. Bryan, and M. W. Hecht (2000), Numerical simulation of the North Atlantic Ocean at 1/10°, *J. Phys. Oceanogr.*, *30*, 1532–1561.

Stevens, D. P. (1990), On open boundary conditions for three dimensional primitiv equation ocean circulation models, *Geophys. Astrophys. Fluid Dyn.*, *51*, 103–133.

Takahashi, T., et al. (2002), Global sea–air CO_2 flux based on climatological surface ocean pCO_2, and seasonal biological and temperature effects, *Deep Sea Res., Part II*, *49*(9–10), 1601–1622.

Wanninkhof, R. (1992), Relationship between gas exchange and wind speed over the ocean, *J. Geophys. Res.*, *97*(C5), 7373–7381.

Wanninkhof, R., and W. R. McGillis (1999), A cubic relationship between air–sea CO_2 exchange and wind speed, *Geophys. Res. Lett.*, *26*(13), 1889–1892.

Wanninkhof, R., S. Doney, T.-H. Peng, J. L. Bullister, K. Lee, and R. A. Feely (1999), Comparison of methods to determine the anthropogenic CO_2 invasion into the Atlantic Ocean, *Tellus, Ser. B*, *51*, 511–530.

Willebrand, J., B. Barnier, C. Böning, C. Dieterich, P. Killworth, C. LeProvost, Y. Jia, J. M. Molines, and A. L. New (2001), Circulation characteristics in three eddy-permitting models of the North Atlantic, *Prog. Oceanogr.*, *48*(2–3), 123–161.

C. Eden, Leibniz Institute for Marine Science at University of Kiel (IFM-GEOMAR), FB I, Düsternbrooker Weg 20, D-24105 Kiel, Germany. (ceden@ifm-geomar.de)

A. Oschlies, National Oceanography Centre, European Way, Southampton S014 3ZH, UK. (azo@noc.soton.ac.uk)